Eur. Phys. J. D **36**, 261–269 (2005)
DOI: 10.1140/epjd/e2005-00243-1

THE EUROPEAN PHYSICAL JOURNAL D

Kerr effect of molecular oxygen at $\lambda = 1064$ nm

Experiment and theory

F. Bielsa[1], R. Battesti[2], C. Robilliard[1], G. Bialolenker[1,3], G. Bailly[1], G. Trénec[1], A. Rizzo[4], and C. Rizzo[1,a]

[1] Laboratoire Collisions, Agrégats, Réactivité, IRSAMC, CNRS/UPS, 31062 Toulouse, France
[2] Laboratoire National des Champs Magnétiques Pulsés, CNRS/UPS/INSA, 31432 Toulouse, France
[3] Nuclear Research Center Negev, 84190 Beer-Sheva, Israel
[4] Istituto per i Processi Chimico Fisici, CNR, 56124 Pisa, Italy

Received 8 March 2005
Published online 30 August 2005 –

Abstract. We report a new measurement of the Kerr effect of molecular oxygen at $\lambda = 1064$ nm. The experimental value reported for the anisotropy of the index of refraction Δn_u^l, $(3.15\pm0.85)\times10^{-25}$ m^2 V^{-2} atm^{-1}, is in good agreement with the value of 3.4×10^{-25} m^2 V^{-2} atm^{-1} obtained via an *ab initio* calculation. We show that the dependence of the effect on the pressure is not linear because of the presence of a collision-induced absorption band around 1060 nm due to the transition from the $X^3\Sigma_g^-$ ground state to the $^1\Delta_g$ state. We also give the value of the quadratic anisotropy Δn_u^q $(-1.03 \pm 0.68) \times 10^{-25}$ m^2 V^{-2} atm^{-2}. We finally compare our *ab initio* theoretical and experimental results with previous existing data.

PACS. 33.55.Fi Other magnetooptical and electrooptical effects – 42.25.Lc Birefringence

1 Introduction

Linearly polarized light passing through a medium in the presence of a transverse electrical field acquires an ellipticity. This is know as Kerr effect (KE) since it was discovered by Kerr in 1875 [1,2]. KE is usually weak, and measurements in gases have been performed only in the past few decades [3].

At the wavelength λ the ellipticity is proportional to the linear birefringence $\Delta n(\lambda, T, E, N) = n_{||} - n_\perp$, where $n_{||}$ is the refractive index for the polarization component parallel to the external electric field and $n_\perp$ the one for the polarization component perpendicular to the field. T is the temperature, E is the strength of the applied electric field and N is the number density ($N = N_a/V_m$, with N_a indicating Avogadro's number and V_m the molar volume). $\Delta n(\lambda, T, E, N)$ is related to the microscopic properties of the sample through the so-called "Kerr constant" ${}_mK(\lambda, T)$, which, for homonuclear diatomic molecules can be written as [4,3]

$$ {}_mK(\lambda, T) = \frac{N_A}{81\epsilon_0}\left[\gamma_K(\omega) + \frac{1}{5kT}\alpha_{ani}(\omega)\alpha_{ani}(0)\right] \quad (1)$$

$\alpha_{\alpha\beta}(0)$ and $\alpha_{\alpha\beta}(\omega)$ indicate the static and frequency dependent electric dipole polarizabilities, respectively, and α_{ani} is their anisotropy, defined as (z is chosen as principal symmetry axis all throughout this paper)

$$\alpha_{ani}(\omega) = \alpha_{zz}(\omega) - \alpha_{xx}(\omega) \quad (2)$$

$\gamma_K(\omega)$ combines dynamic second electric dipole hyperpolarizability tensor components [5], $\gamma_{\alpha\beta\gamma\delta}(-\omega;\omega,0,0)$, in a shortened notation indicated as $\gamma_{\alpha\beta\gamma\delta}(\omega)$,

$$\gamma_K(\omega) = \frac{1}{10}\Big[3\gamma_{\xi\eta\xi\eta}(\omega) - \gamma_{\xi\xi\eta\eta}(\omega)\Big]. \quad (3)$$

Einstein summation over repeated indices is assumed here and elsewhere. By exploiting the symmetry relationships, dictating the relationships existing between the different tensor components of $\gamma(\omega)$ and the number of non vanishing elements [6], again for homonuclear diatomics equation (3) simplifies into

$$\gamma_K(\omega) = \frac{1}{5}\Big[\gamma_{xxyy} - \gamma_{xxzz} + 7\gamma_{xyyx} + 6\gamma_{zxxz} - \gamma_{zzxx} + \gamma_{zzzz}\Big]. \quad (4)$$

The frequency argument is sometimes omitted for ease of notation above and in the following.

The anisotropy of the refractive index for the molecule considered here then becomes

$$\Delta n(\lambda, T, E, N) = \frac{2\pi E^2 N_A}{3V_m(4\pi\epsilon_0)}\Big[\gamma_K(\omega) + \frac{1}{5kT}\alpha_{ani}(\omega)\alpha_{ani}(0)\Big] = \frac{27E^2}{2V_m}\ {}_mK(\lambda, T). \quad (5)$$

[a] e-mail: carlo.rizzo@irsamc.ups-tlse.fr

In equations (1) and (5) and in the following k is the Boltzmann constant. For ideal gases, indicating with P the pressure,

$$\Delta n(\lambda, T, E, P) \approx \frac{2\pi E^2 P}{3kT(4\pi\epsilon_0)}\left[\gamma_K(\omega) + \frac{1}{5kT}\alpha_{ani}(\omega)\alpha_{ani}(0)\right]. \quad (6)$$

From the values of γ and α given in atomic units the expression for ${}_mK(\lambda, T)$, computed in SI, becomes

$${}_mK(\lambda, T) = 5.23576 \times 10^{-32} \times \left[\gamma_K(\omega) + \frac{63154.93}{T}\alpha_{ani}(\omega)\alpha_{ani}(0)\right] \quad (7)$$

with E given in V m^{-1}, the pressure in atm, the temperature in K and the quantity within square brackets in au, equation (6) above is rewritten as

$$\Delta n(\lambda, T, E, P) = \frac{8.61382 \times 10^{-27} \times (E[\mathrm{Vm}^{-1}])^2 \times P[\mathrm{atm}]}{T[\mathrm{K}]} \times \left[\gamma_K(\omega) + \frac{1}{5kT}\alpha_{ani}(\omega)\alpha_{ani}(0)\right][\mathrm{au}]. \quad (8)$$

The KE of molecular oxygen was measured by Carusotto et al. in 1985 at $\lambda = 514.5$ nm [7], and more recently by Inbar and Arie at $\lambda = 1064$ nm [8]. In reference [8] a measurement at the same wavelength, published in 1982 by Mak et al., is mentioned [9], whereas in reference [7] the value at $\lambda = 650$ nm published in 1936 by Breazeale is reported [10]. The estimates of Carusotto et al. [7] and Breazeale [10] are given with a few percents error bars whereas the measurements at $\lambda = 1064$ nm [8,9] are affected by a relative error larger than 50%. Measurements at this wavelength are somewhat complicated by the presence of an absorption band around 1060 nm. This is due to the transition from the $X^3\Sigma_g^-$ ground state to the $^1\Delta_g$ state, starting from the $v = 0$ of the ground state to the $v = 1$ of the excited state. Experimental absorption spectra can be found in references [11–13], while a theoretical analysis can be found in [14].

As for theoretical prediction of the KE of molecular oxygen, *ab initio* calculations of the static and dynamic electric dipole polarizability have been performed in several instances and at different levels of accuracy, see for instance [15–21]. One of the present authors was involved in a study of these properties in conjunction with the analysis of Cotton–Mouton effect [22–24] of molecular oxygen, see reference [25]. The second electric dipole hyperpolarizability has been visited much less often, and we are aware only of the study carried out for the static tensor $\gamma(0; 0, 0, 0)$ by Neogrády and co-workers [21] and of that for dc-Second Harmonic Generation (dc-SHG) $\gamma(-2\omega; \omega, \omega, 0)$ by Luo and his collaborators [17], see reference [26].

In this paper we report the results of a new measurement of the KE of molecular oxygen performed at $\lambda = 1064$ nm and at room temperature, and compare them with the *ab initio* estimate. Our data clearly show that, due to absorption, the Kerr effect of O_2 around $\lambda = 1064$ nm does not increase linearly with the gas pressure and at least a quadratic term has to be introduced in the power expansion. In the limit of low pressure our data are in good agreement with the result of *ab initio* calculations.

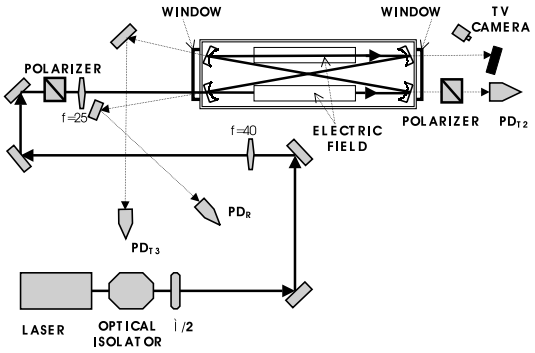

Fig. 1. Drawing of the apparatus.

2 Experimental methods

Our apparatus is based on a ring cavity to which a Nd:YAG laser was frequency locked. Using a resonant optical cavity, we increased the effect of a round trip of the light in electric field region by a factor $\alpha \sim 2000$. A schematic drawing of the apparatus is given in Figure 1.

The light source is a tunable non planar ring oscillator Nd:YAG laser emitting $\sim$ 200 mW of power at a wavelength $\lambda = 1064$ nm ($\nu = 2.82 \times 10^{14}$ Hz). The frequency of the laser can be changed by two methods: a fast one (bandwidth > 1 Hz) based on a piezoelectric actuator acting on the laser crystal and a slow one (bandwidth < 1 Hz) based on the change of the crystal temperature. In practice, the former allows to vary the laser frequency of about 50×10^6 Hz, whereas the latter yields changed of about 100×10^9 Hz.

The laser light, after crossing a two-stage optical isolator, goes through a half-wave plate used to change the polarization direction of the beam. Mirrors for 45° incidence are used to transport the beam and to properly align the beam and the cavity. Two lenses ($f = 40$ cm and $f = 25$ cm) are used to match the waist of the beam with the waist of the cavity. The laser light is linearly polarized by using a polarizer prism before entering the cavity region and is analyzed by using another polarizer prism placed beyond the cavity region.

Photodiode PD_R is used to detect light reflected by the cavity. This detector can provide a DC signal used to align the photodiode itself and an AC-coupled signal fed into the electronics and devoted to the locking of the laser to the cavity.

The servo system used to lock the laser to the ring cavity is based on the Drever-Hall technique [27]. FM sidebands were generated by direct modulation of the piezo transducer attached to the NPRO crystal [28].

Photodiode PD_{T2} is used to measure, after the analyzer prism, the intensity of the light transmitted by the second cavity mirror. Photodiode PD_{T3} is employed to monitor the intensity of the light transmitted by the third cavity mirror and it is used as a reference for the light coupled to the cavity. The signal of PD_{T2}, when the analyzer prism is set to maximum extinction, is sent to a spectrum analyzer to detect the Kerr signal in phase with the modulation of the electric field. A TV camera is used to monitor the TEM_{00} cavity mode focusing on the beam transmitted by the forth mirror.

To enter and exit the cavity region light passes through quartz windows with antireflection coating for $\lambda = 1064$ nm. The cavity is contained in a vacuum chamber [29] that can be evacuated using a dry pump and filled with gas. The gas sample used in our study was pure at 99.995%. Pressure was measured using a mechanical gauge (not shown in the drawing). Measurements were conducted at room temperature.

The cavity itself is made by four identical high reflectivity mirrors, provided by Newport Inc. (type Supermirrors, radius of curvature = 1 m), and designed to provide a finesse higher than 10 000 in a linear cavity and therefore a finesse higher than 5 000 in our four identical mirror ring cavity. Mirrors are for 0° incidence. Our ring cavity was designed to minimize the incidence angle on the mirrors ($i \sim 3°$) and therefore to minimize the birefringence given by non 0° incidence angles. We obtained the cavity finesse by measuring the decay time τ of the intensity signal of PD_{T3} once the laser had been switched to stand-by position. The decay time of the stand-by switch itself was measured to be about 0.5 μs. The cavity finesse F is related to the intensity decay time τ of our ring cavity by the formula $F/\pi = 2c_0\tau/L$, where c_0 is the velocity of light and L the length of a round trip in the cavity. In our case L was 2.439 m. We measured a decay time of ≈8.0 μs, corresponding to finesse of ≈6000. No dependence of cavity finesse on the polarization direction of light was observed.

The value of the ratio between the light intensity transmitted by one of the cavity mirror and the light intensity injected into the cavity η was about 10%. Decay time and light intensity transmitted in O_2 depend on the gas pressure, an effect due to absorption of molecular oxygen at $\lambda \approx 1060$nm. This effect will be discussed later.

The transverse electric field E was provided by two electrodes, 275 mm long, separated by 5 mm and driven by a high voltage supply amplifier. Two electric field regions were present inside the ring cavity. The maximum electric field used during measurements was about 280 000 V m^{-1}. In order to apply a homodyne technique for the signal detection the electric field was modulated at a frequency of 11 Hz. To determine the electric field amplitude at the main 11 Hz harmonic and to monitor DC contribution and higher frequency harmonics, the voltage was measured directly on the electrodes and analyzed by a Fourier spectrum.

KE could also be observed using a linear cavity [8]. We have developed an apparatus based on a ring cavity because ring cavities are of more general application and could be used also to observe other magneto-electric effects that cannot be amplified in a linear cavity due to their symmetry properties [30].

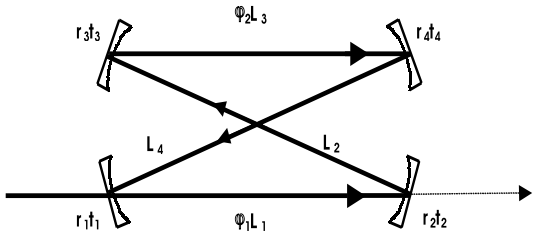

Fig. 2. Schematic drawing of the ring cavity.

2.1 Our ring cavity in a birefringent and absorbing medium

In this paragraph, we derive some formulas that will be used in the following data analysis. The ring cavity is sketched in the scheme of Figure 2.

The intensity of light exiting the ring cavity through mirror 2 can be calculated by writing the Jones matrix [31] $\mathbf{t}_2$:

$$\mathbf{t}_2 = \sum_{n=0}^{\infty} t_1 \left[\begin{pmatrix} e^{i\frac{\varphi_1}{2}} & 0 \\ 0 & e^{-i\frac{\varphi_1}{2}} \end{pmatrix} e^{-\alpha L_1} r_2 e^{-\alpha L_2} r_3 \right]^n \times \left[\begin{pmatrix} e^{i\frac{\varphi_2}{2}} & 0 \\ 0 & e^{-i\frac{\varphi_2}{2}} \end{pmatrix} e^{-\alpha L_3} r_4 e^{-\alpha L_4} r_1 \right]^n \times \begin{pmatrix} e^{i\frac{\varphi_1}{2}} & 0 \\ 0 & e^{-i\frac{\varphi_1}{2}} \end{pmatrix} e^{-\alpha L_1} t_2. \quad (9)$$

In our case, $L_1 + L_2 + L_3 + L_4 = L$, L standing for the length of a round trip in the cavity; $\varphi_1 = \varphi_2$, $\varphi_1 + \varphi_2 = \varphi$ with φ as the total phase acquired by the light in the electric field; $r_1 = r_2 = r_3 = r_4 = r$; $t_1 = t_2 = t_3 = t_4 = t$; $R = r^2$ and $T = t^2$ where R and T are the mirror intensity reflectivity and transmission, respectively. Therefore

$$\mathbf{t}_2 = \sum_{n=0}^{\infty} T \left[e^{-\alpha L} R^2 \begin{pmatrix} e^{i\frac{\varphi}{2}} & 0 \\ 0 & e^{-i\frac{\varphi}{2}} \end{pmatrix} \right]^n \times \begin{pmatrix} e^{i\frac{\varphi}{4}} & 0 \\ 0 & e^{-i\frac{\varphi}{4}} \end{pmatrix} e^{-\alpha L_1}. \quad (10)$$

Matrix algebra yields

$$\mathbf{t}_2 = \frac{T e^{-\alpha L_1}}{1 - R^2 e^{-\alpha L}} \times \begin{pmatrix} e^{i\left(\frac{1}{2}\frac{1+R^2 e^{-\alpha L}}{1-R^2 e^{-\alpha L}}\right)\frac{\varphi}{2}} & 0 \\ 0 & e^{-i\left(\frac{1}{2}\frac{1+R^2 e^{-\alpha L}}{1-R^2 e^{-\alpha L}}\right)\frac{\varphi}{2}} \end{pmatrix}. \quad (11)$$

Since αL_1, $\alpha L \ll 1$

$$\mathbf{t}_2 = \frac{T}{(1-R^2)+\alpha L R^2} \times \begin{pmatrix} e^{i\left[\frac{1}{2}\frac{1+R^2}{(1-R^2)+\alpha L R^2}\right]\frac{\varphi}{2}} & 0 \\ 0 & e^{-i\left[\frac{1}{2}\frac{1+R^2}{(1-R^2)+\alpha L R^2}\right]\frac{\varphi}{2}} \end{pmatrix}. \quad (12)$$

The ring cavity finesse over π can be written as

$$\frac{F}{\pi} = \frac{1}{(1-R^2)+\alpha L R^2} \quad (13)$$

and, since $R \approx 1$ and $R^2 \approx 1$,

$$\frac{F}{\pi} = \frac{1}{2(1-R)+\alpha L}. \quad (14)$$

Therefore the birefringence φ corresponding to a round trip in the cavity is amplified by a factor

$$g = \frac{1}{2}(1+R^2)\frac{F}{\pi} \approx \frac{F}{\pi}. \quad (15)$$

In our case α is mainly proportional to the square of the pressure P [11].

As far as the intensity decay time τ is concerned, this is, as usual, half the field decay time since the intensity is the square of the field

$$\tau = \frac{1}{2}\frac{F}{\pi}\frac{L}{c}. \quad (16)$$

Finally, the intensity transmitted by the cavity mirror #2 I_2 can be written as

$$I_2 = I_0\left(\frac{TF}{\pi}\right)^2. \quad (17)$$

Due to absorption in the gas, τ and I_2 depends on the pressure P. It is straightforward to show that $I_3 \approx I_2$.

2.2 Homodyne detection technique

The light intensity $I(t)$ incident on the photodiode PD_{T2} with the analyzer crossed at maximum extinction can be written as

$$\begin{aligned} I(t) &= I_2\{\sigma^2 + [\Gamma + \psi(t)]^2\} \\ &= I_2[\sigma^2 + \Gamma^2 + 2\Gamma\psi(t) + \psi(t)^2] \end{aligned} \quad (18)$$

where σ^2 is the extinction factor given by the pair polarizer-analyzer. Typically $\sigma^2 \sim 10^{-7}$. Γ is a static ellipticity and it is due to the cavity mirrors and to the vacuum chamber quartz windows. The ellipticity of the mirrors has two origins: the intrinsic birefringence of the reflecting layers of the interferential mirrors (see e.g. [32]) and non zero incidence angle birefringence [33]. Γ acts as the DC carrier in our homodyne detection scheme. $\Gamma \simeq 0.08$ and therefore $\sigma^2 \ll \Gamma^2$.

$\psi(t)$ is the effect to be measured. With our experimental parameters, $\psi(t)$ is of the order $10^{-5} \div 10^{-6}$. Because of the periodic modulation of the electric field, $\psi(t)$ can be written as

$$\psi(t) = g \times \pi\frac{L_E}{\lambda}\Delta n_u(\lambda, T, P)E(t)^2 \quad (19)$$

where L_E is the length of the total electric field region and $\Delta n_u(\lambda, T, P)$ is the Kerr anisotropy for an electric field of 1 V m^{-1} at pressure P. In our case $E(t) = E_0\cos(2\pi\nu_E t)$, with $\nu_E = 11$ Hz we have taken the electric field phase as the zero reference phase. Thus

$$E(t)^2 = [E_0\cos(2\pi\nu_e t)]^2 = \frac{E_0^2}{2}[1+\cos(2\pi(2\nu_E)t)]. \quad (20)$$

The Fourier spectrum of the signal includes two relevant components. A DC component I_{DC} and a component at $2\nu_E$ $I_{2\nu_E}$

$$\begin{aligned} I_{DC} &= I_2\Gamma^2 \\ I_{2\nu_E} &= I_2 F\frac{L_E}{\lambda}\Delta n_u(\lambda, T, P)E_0^2\Gamma. \end{aligned} \quad (21)$$

Finally

$$\Delta n_u(\lambda, T, P) = \frac{\lambda I_{2\nu_E}}{FL_E E_0^2\sqrt{I_{DC}I_2}}. \quad (22)$$

3 Computational methods and results

3.1 The method and the effect of molecular vibrations

We studied computationally the KE of oxygen, by resorting to analytical linear (for the electric dipole polarizability anisotropies) and cubic (for the hyperpolarizability contribution) frequency dependent response theory [34,35]. In particular, we have employed multiconfigurational self-consistent field (MCSCF) response [34,35], following closely the procedure adopted in reference [25]. The electronic frequency-dependent electric dipole polarizability and dc-Kerr second hyperpolarizability γ_K were computed at three frequencies corresponding to wavelengths λ of 514.5 nm, 632.8 nm and 1064.0 nm and at the equilibrium internuclear distance using a rather large complete active space, see details below. In our approach, where electronic and nuclear motions are treated separately, we have to consider that molecular vibrations also contribute to the overall property. Their effect, which in a first approximation can be decoupled from that of electrons and added to the equilibrium electronic property, involves both a zero-point averaging (ZPVA) and the determination of the so-called pure vibrational second hyperpolarizability γ_K^{pv} [36–38]. For property A ($A = \alpha_{ani}$ or γ_K in our case)

$$A = A^e(Q_e) + \Delta A^{ZPVA} + A^{pv} \quad (23)$$

where $A^e(Q_e)$ is the electronic property evaluated at the (fixed) equilibrium geometry R_e, ΔA^{ZPVA} is the correction due to zero-point vibrational averaging of the electronic property

$$\Delta A^{ZPVA} = \langle \psi_0 \mid A^e(Q) \mid \psi_0 \rangle - A^e(Q_e). \quad (24)$$

Here ψ_0 is the ground-state vibrational wave function. $Q = \sqrt{\mu}(R - R_e)$ is the normal coordinate, with μ as reduced nuclear mass, R as the inter-nuclear distance, and R_e the equilibrium field-free bond length. A^{pv} denotes the so-called pure vibrational contribution. For O_2

$$\gamma^{pv}_{\alpha\beta\gamma\delta}(-\omega_\sigma;\omega_1,\omega_2,\omega_3) = \frac{1}{4\hbar}\sum \mathcal{P}_{\alpha\beta\gamma\delta}\sum_{k\neq 0}\frac{(\alpha^e_{\alpha\beta})_{0k}(\alpha^e_{\gamma\delta})_{k0}}{\omega_k - \omega_2 - \omega_3} \quad (25)$$

$|\psi_k\rangle$ being the kth fundamental vibrational wave function, with energy $\hbar\omega_k$, whereas $\sum \mathcal{P}_{\alpha\beta\gamma\delta}$ indicates summation over the terms obtained by permuting the pairs $(-\omega_\sigma, \alpha)$, (ω_1, β), (ω_2, γ) and (ω_3, δ) (α, β, γ, $\delta = x, y, z$, $\omega_\sigma = \omega_1 + \omega_2 + \omega_3$). $(\alpha^e_{\alpha\beta})_{0k} = \langle \psi_0 \mid \alpha^e_{\alpha\beta}(Q) \mid \psi_k \rangle$. There are no pure vibrational contributions to the anisotropy of the electric dipole polarizability α_{ani} for non-dipolar molecules as O_2.

To obtain these corrections, the relevant electronic properties (electric dipole polarizabilities and hyperpolarizabilities) are computed at a few inter-nuclear distances around the equilibrium distance, and the ro-vibrational averages are calculated, once a suitable potential energy curve for the electronic ground state is made available.

3.2 Computational details

Calculations were performed using Dunning's [39,40] d-aug-cc-pVQZ correlation consistent basis set. It includes 210 basis functions, and it is composed of $14s8p5d4f3g$ uncontracted functions contracted to a $7s6p5d4f3g$ set. Some results were also obtained with the smaller d-aug-cc-pVTZ basis set, a $[12s7p4d3f\ |6s5p4d3f]$, 124 contracted functions basis sets. The results obtained with this set were used to analyze the degree of convergence with the quality of the expansion set yielded by our larger set. This was considered to be adequate for the degree of accuracy we are aiming in this study.

Two different complete active space SCF (CASSCF) reference wave functions [41] were employed in the multiconfigurational cubic response calculations. The number of inactive and active orbitals is given in the following with reference to the irreducible representations of the D_{2h} subgroup of the full $D_{\infty h}$ group: the notation $(n_1\ n_2\ \cdots n_8)$ indicates the number of orbitals in the $\sigma_g\ \pi_{ux}\ \pi_{uy}\ \delta_g\ \sigma_u\ \pi_{gx}\ \pi_{gy}$ and δ_u symmetries respectively:

CAS-I inactive (2 0 0 0 1 0 0 0)
active (2 2 2 0 2 1 1 0);

CAS-II inactive (2 0 0 0 1 0 0 0)
active (3 3 3 1 3 2 2 0).

CAS-I includes the $2\sigma_u, 3\sigma_g, 1\pi_u, 1\pi_g, 3\sigma_u, 4\sigma_g$ and $2\pi_u$ orbitals, and with respect to the usually employed so-called Full-Valence CAS, it only excludes the $2\sigma_g$ orbital — which is a truly "inactive" orbital — while including the $4\sigma_g$ and the $2\pi_u$ orbitals. CAS-I was employed for the calculations needed to determine the effect of molecular vibrations on the equilibrium electronic properties. CAS-II is far larger, yielding more than two million variables in the CASSCF optimization, and it was employed to obtain the values of the properties at the equilibrium distance, which was taken to be the experimental one, 2.28167 au [42].

The potential energy curve of the ground $X^3\Sigma_g^-$ state of oxygen, needed to perform the rotational and vibrational averaging of the electronic properties, was taken from experiment [43]. We also determined a non relativistic curve for the $X^3\Sigma_g^-$ state of O_2 in the same range of internuclear distances employed for the calculation of the properties, see just below, but, owing to the relatively small CAS employed in these calculations (CAS-I), it was considered more adequate to resort to the experimental curve for our averaging procedure. The electric properties were then computed at the equilibrium internuclear distances and at twenty more distances, equally spaced between 1.000095 and 1.570149 Å, for a wavelength of 632.8 nm, with the d-aug-cc-pVQZ basis set and CAS-I. Zero point vibrational averages and the matrix elements of the electronic properties between the lowest eight vibrational levels supported by the experimental potential curve, and, for each vibrational state, between the lowest seven rotational sublevels, were computed using VIBROT, which is part of the MOLCAS program suite [44]. All the other calculations were performed using the DALTON program [45].

3.3 Ab initio analysis

The computational results are summarized in Tables 1, 2, 3 and 4. The former includes the fixed equilibrium geometry estimates obtained for the properties contributing to the expression of the Kerr constant, equation (1). These are the electric dipole polarizability anisotropy, equation (2), and the dc-Kerr second electric dipole hyperpolarizability, equation (3). The data are then employed to obtain estimates for the electronic Kerr constant at a temperature of 295.15 K (room temperature), and at the same temperature the birefringence per unit electric field and a pressure of 1 atm, denoted $\Delta n_u(\lambda, T)$.

Our best estimate for the average electric dipole polarizability $\alpha_{ave} = (2\alpha_{xx} + \alpha_{zz})$ for $\lambda = 632.8$ nm is 10.66 au, to be compared with the value of 10.723 obtained by Spelsberg and Mayer [19] and that derived from the experimental depolarization ratio of Bridge and Buckingham [46], 10.78 au. For the anisotropy Spelsberg and Meyer obtain a value of 7.238 au, in nice agreement with our 7.2745 au, see Table 1. As far as the static values are concerned, Neogrády and co-workers [21] suggested as recommended *ab initio* estimate — obtained using a

Table 1. O_2. Electric dipole polarizability anisotropy $\alpha_{ani}(\omega)$, dc-Kerr second dipole hyperpolarizability $\gamma_K(\omega)$, Kerr constant ${}_mK(\lambda,T)$ and birefringence measured for a field of 1 Vm^{-1} and a pressure of 1 atm, $\Delta n_u(\lambda,T)$, obtained at three different wavelengths for a temperature T of 295.15 K. Fixed nuclei at the (experimental) equilibrium geometry. The static electric dipole anisotropy is computed (again with MCSCF response and CAS-II) to be $\alpha_{ani}(0)$ is 6.9915 au. All results obtained with the d-aug-cc-pVQZ basis set, with MCSCF response using CAS-II, see text. SI units for ${}_mK$ are V^{-2} m^5 mol^{-1}. Δn_u is given in units of m^2 V^{-2} atm^{-1}.

λ nm	$\alpha_{ani}(\omega)$ au	$\gamma_K(\omega)$ au	${}_mK(\lambda,T)$ SI units $\times 10^{28}$	$\Delta n_u(\lambda,T)$ SI units $\times 10^{25}$
514.5	7.4310	899.29	6.29	3.51
638.8	7.2745	868.42[(a)]	6.16	3.43
1064.0	7.0885	832.32	5.99	3.34

[(a)] Cf. $\gamma_K(\omega) = 655$ a.u. with MCSCF response, CAS-I.

Table 2. O_2. The computed Kerr constant ${}_mK(\lambda,T)$ (in SI units $\times 10^{28}$) as a function of the temperature T (in K) for three wavelengths (in nm). Fixed nuclei at the (experimental) equilibrium geometry. Results obtained with the d-aug-cc-pVQZ basis set, with MCSCF response using CAS-II, see text.

	λ		
T	514.4	632.8	1064.0
273.15	6.76	6.61	6.44
283.15	6.54	6.39	6.22
293.15	6.33	6.19	6.03
300.00	6.20	6.06	5.90
303.15	6.14	6.00	5.84
313.15	5.96	5.83	5.67
323.15	5.79	5.66	5.51

Table 3. O_2. The results of the study of the vibrational contributions to the electric dipole polarizability anisotropy α_{ani} and the dc-Kerr second dipole hyperpolarizability $\gamma_K(\omega)$ obtained for $\lambda = 632.8$ nm. d-aug-cc-pVQZ basis set, with MCSCF response using CAS-I. The ZPVA is computed by averaging over the lowest eight vibrational states of the experimental ground $X^3\Sigma_g^-$ state potential curve of O_2, including seven rotational sublevels per vibrational state. The values given in the table are for an average temperature between 273.15 and 293.15 K. To compute the pure vibrational a sum over the same eight lowest vibrational states was performed, see equation (25). Atomic units.

	$\alpha_{ani}(0)$	$\alpha_{ani}(\omega)$	$\gamma_K(\omega)$
$P^e(Q_e)$	6.7544	7.0519	654.70
$\langle\psi_0 \mid P^e(Q) \mid \psi_0\rangle$	6.8772	7.1919	671.79
ΔP^{ZPVA}	0.1228	0.1400	17.09
P^{pv}			217.08
P	6.8772	7.1919	888.87

Table 4. O_2. Estimated electric dipole polarizability anisotropy α_{ani}, dc-Kerr second dipole hyperpolarizability $\gamma_K(\omega)$, Kerr constant ${}_mK(\lambda,T)$ and birefringence measured for a field of 1 Vm^{-1} and a pressure of 1 atm $\Delta n_u(\lambda,T)$, at three different wavelengths for a temperature T of 295.15 K. Value obtained from those of Table 1, assuming percentage increase due to ZPVA and (for the hyperpolarizability) pure vibrational contribution as computed using the d-aug-cc-pVQZ basis set, CAS-I and neglecting the frequency dispersion. SI units for ${}_mK$ are V^{-2} m^5 mol^{-1}. Δn_u is given in units of m^2 V^{-2} atm^{-1}.

λ nm	$\alpha_{ani}(0)$ au	$\alpha_{ani}(\omega)$ au	$\gamma_K(\omega)$ au	${}_mK(\lambda,T)$ SI $\times 10^{28}$	$\Delta n_u(\lambda,T)$ SI $\times 10^{25}$
514.5	7.12	7.58	1221	6.7	3.7
638.8	7.12	7.42	1179	6.5	3.6
1064.0	7.12	7.23	1130	6.4	3.5

spin-adapted CCSD(T) complete basis set limit, including core correlation, vibrational and relativistic correction — values of $\alpha_{ave}(0) = 10.46$ au and $\alpha_{ani}(0) = 6.85$ au. The corresponding experimental estimates, obtained from dipole oscillator strength distributions [47,48], are 10.59 au and 7.05 au, respectively. With MCSCF response and CAS-II, we obtain 10.49 au for the average and 6.99 for the anisotropy. To our knowledge, there are no other calculated values of the Kerr hyperpolarizability $\gamma_K(\omega)$ of oxygen in the literature to compare our results with.

The temperature dependence of the Kerr constant as computed with our best basis set and best CAS is shown in Table 2. The results of our analysis of the vibrational contribution to the electronic properties are reported in Table 3. It can be seen that, using the d-aug-cc-pVQZ and the relatively contained CAS-I complete active space, for a wavelength of 632.8 nm, the electronic estimates obtained at the (experimental) equilibrium internuclear distance increase due to ZPVA by 1.82%, 1.98% and 2.61% for $\alpha_{ani}(0)$, $\alpha_{ani}(\omega)$ and $\gamma_K(\omega)$, respectively. The pure vibrational contribution to the dc-Kerr second electric dipole hyperpolarizability $\gamma_K(\omega)$ is as large as 33% of the electronic value. When using the $X^3\Sigma_g^-$ potential energy curve computed with the d-aug-cc-pVQZ basis set and CAS-I, the percentages are noticeably higher for the ZPVA, between 4% and 5% increase for $\alpha_{ani}(0)$, $\alpha_{ani}(\omega)$ and $\gamma_K(\omega)$, whereas the size of the pure vibrational contribution to $\gamma_K(\omega)$ is of about 36% the electronic value. Including the effect of molecular vibrations, the estimate of the Kerr constant of O_2 at 632.8 nm, a temperature of 295.15 K, as obtained using the d-aug-cc-pVQZ basis set and the smaller complete active space employed in this study (CAS-I), changes from 5.68×10^{-28} V^{-2} m^5 mol^{-1} to 6.01×10^{-28} V^{-2} m^5 mol^{-1}. The birefringence goes from 3.17×10^{-25} m^2 V^{-2} atm^{-1} to 3.35×10^{-25} m^2 V^{-2} atm^{-1}.

The direct calculation of the properties $A(Q)$, for the electric polarizability tensor as well as for the dc-Kerr second electric dipole hyperpolarizability, using the larger complete active space, CAS-II, with the d-aug-cc-pVQZ basis set was not attempted, as the computational cost is nowadays still far larger than the acceptable for the accuracy we can achieve in the analysis. We used instead the results of the vibrational study given in Table 3, and assumed that the increase, due to the effect of ZPVA for the

properties remains percent-wise the same when increasing the complete active space, and is independent of the frequency. We thus added to the equilibrium values of the properties given in Table 1, a contribution corresponding to percentages equal to 1.82, 1.98 and 2.61, respectively, for $\alpha_{ani}(0)$, $\alpha_{ani}(\omega)$ and $\gamma_K(\omega)$. Furthermore, to account for γ_K^{pv}, we added a contribution to $\gamma_K(\omega)$ equal to ≈33.2% of the original electronic fixed equilibrium geometry value. The results of this procedure are shown in Table 4. Our final *ab initio* estimate for the Kerr constant of molecular oxygen at 1064.0 nm and a temperature of 295.15 K (room temperature) is thus ${}_mK(\lambda = 1064$ nm, $T = 295.15$ K$) = 6.4 \times 10^{-28}$ V^{-2} m^5 mol^{-1}. The birefringence per unit electric field per atmosphere, again at 295.15 K, is estimated to be $\Delta n_u(\lambda = 1064$ nm, $T = 295.15$ K$) = 3.5 \times 10^{-25}$ m^2 V^{-2} atm^{-1}.

4 Experimental results

Kerr measurements reported here have been performed at different pressures between 0.247 and 0.938 atm. At every pressure we have measured the intensity decay time τ, the intensity I_2, the ratio $k = I_2/I_3$. When the analyzer was set at maximum extinction, once k was known, the value of I_2 could be recovered by measuring I_3.

Because of the absorption band around 1060 nm, values of I_2 decreased by about 30% going from zero to 1 atm pressure while τ values decreased of about 15% in the same range. This is in agreement with the equations (13), (16), (17) and the estimated value of the absorption coefficient and its dependence with the pressure were also compatible with the findings of references [11,12]. At 0.79 atm and room temperature, the absorption coefficient value given in reference [11] corresponds to about 5×10^{-5} m^{-1}.

Once the chamber was filled at a given pressure, we performed different measurements of Kerr effect. Electric field amplitude ranged between a minimum value E_{min} and a maximum value E_{max}, the value of which depended on the pressure. E_{min} was about 140 000÷150 000 V m^{-1} and it was chosen so that the signal component $I_{2\nu_E}$ was at least twice the noise floor around the $2\nu_E$ frequency. E_{max} was chosen by monitoring the current output of the high voltage supply used to drive the electrodes providing the electric field. Optimal working condition corresponds to zero current output. Fields higher than E_{max} gave current output different from zero. This increase of current output was due to discharges in the gas. We also observed that experimental points taken at a field higher than E_{max} showed a bigger Kerr effect with respect to the experimental points taken at a field smaller than E_{max}. Our data are consistent with a linear dependence of E_{max} with the pressure. The maximum value for E_{max} was about 280 000 V m^{-1}.

Measurements were performed by Fourier analyzing the signal coming from PD_{T2} with the two polarizers crossed at maximum extinction. In Figure 3 we show one of the Fourier spectra that were taken. Experimental conditions were $P = 0.642$ atm, $E_0 = 202\,700$ V m^{-1}, $2\nu_E = 22$ Hz, integration time about 100 s. The

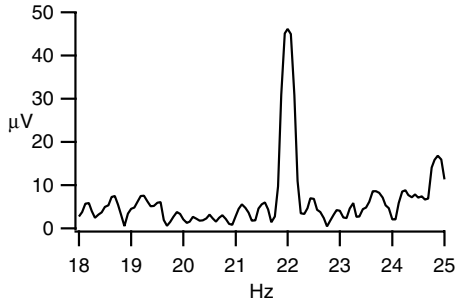

Fig. 3. Fourier spectrum at $P = 0.642$ atm, $E_0 = 202\,700$ V m^{-1}.

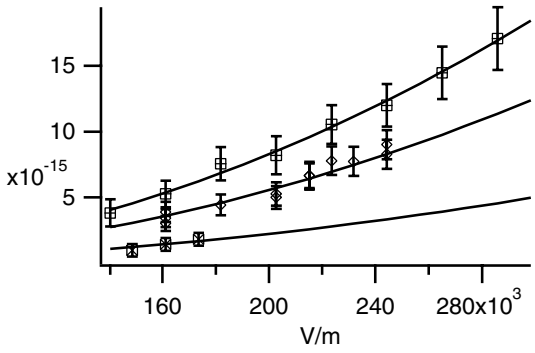

Fig. 4. Data taken at 0.247, 0.642 and 0.840 atm.

peak shown in Figure 3 corresponds to a $\Delta n(\lambda, T, E, P)$ value of $5{\times}10^{-15}$. In general the sensitivity was about $2{\times}10^{-15}$ $1/\sqrt{\text{Hz}}$. The phase of the $I_{2\nu_E}$ signal has also been measured giving values compatible with zero with respect with the phase of the electric field modulation. The sign of the values of $\Delta n(\lambda, T, E, P)$ was found to be positive, as expected.

For any Fourier spectrum taken we have calculated the corresponding $\Delta n_u(\lambda, T, P)$ using formula (22). The final value of $\Delta n_u(\lambda, T, P)$ at a given pressure was obtained by calculating the weighted average of all the experimental values. For calculating the error we used the usual weighted standard deviation.

In Figure 4 we show data taken at 0.247, 0.642 and 0.840 atm. At every pressure, to guide the eyes, we superimposed to the data the curve corresponding to the product $\Delta n_u(\lambda, T, P) \times E_0^2$. The smallest $\Delta n(\lambda, T, E, P)$ measured is about 1×10^{-15} with a noise level corresponding to 4×10^{-16}.

Finally in Figure 5, we plotted the different values of $\Delta n_u(\lambda, T, P)$ as a function of pressure.

We tried first to fit data with the linear function

$$\Delta n_u(\lambda, T, P) = a + bP. \tag{26}$$

The value of the parameter a is expected to be zero within the error. Our data do not display this behavior. This confirms that the presence of the absorption band cannot be disregarded. Fitting data with a quadratic function

$$\Delta n_u(\lambda, T, P) = a + bP + cP^2 \tag{27}$$

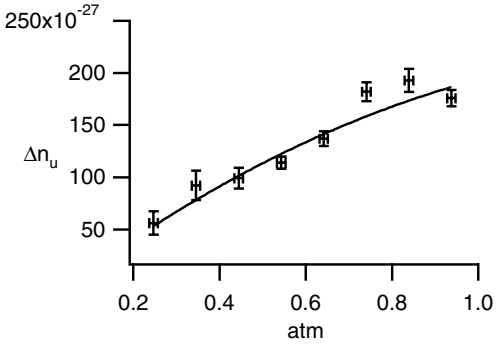

Fig. 5. $\Delta n_u(\lambda, T, P)$ values vs. pressure.

we obtained a value of a compatible with zero, $a = (-1.8 \pm 2.5) \times 10^{-26}$ m^2 V^{-2}. The b and c coefficients yield the linear and quadratic dependence of the effect with the pressure. The corresponding curve is superimposed to the experimental data in Figure 5.

We thus both a linear Kerr effect coefficient Δn_u^l and a quadratic Kerr effect coefficient Δn_u^q

$$\Delta n_u^l = (3.15 \pm 0.85) \times 10^{-25}\,\mathrm{m^2 V^{-2} atm^{-1}} \quad (28)$$

$$\Delta n_u^q = (-1.03 \pm 0.68) \times 10^{-25}\,\mathrm{m^2 V^{-2} atm^{-2}}. \quad (29)$$

5 Comparisons and conclusions

Let's first of all stress that the experimental value of $\Delta n_u^l = (3.15 \pm 0.85) \times 10^{-25}$ m^2 V^{-2} atm^{-1} is in good agreement with the theoretical estimate $\Delta n_u(\lambda = 1064.0$ nm, $T = 295.15$ K$) = 3.5 \times 10^{-25}$ m^2 V^{-2} atm^{-1}. Nevertheless, the experimental precision obtained is limited by the fact that the data exhibit a complicate dependence on the pressure. On the other hand we also give the value $\Delta n_u^q = (-1.03 \pm 0.68) \times 10^{-25}$ m^2 V^{-2} atm^{-2}. A theoretical prediction of the coefficient expressing the deviation for the linearity on the relationship between KE and pressure requires the calculation of energy and property surfaces of two interacting molecules of oxygen, and the calculation of complicate semi-classical integrals [4]. This is both beyond the possibilities and the scope of the present study. Such an analysis has been carried out for rare gases in references [49–51].

The Kerr effect of oxygen has been measured a few times, see Introduction. The more recent value at $\lambda = 1064$ nm has been given by Inbar and Arie in reference [8]. They measured a ratio of the Kerr effect of CO_2 and O_2 at 1 atm and 300 K of (3.16 ± 1.41) and a Kerr anisotropy for CO_2 of $(2.08 \pm 0.66) \times 10^{-24}$ m^2 V^{-2}. Thus one can estimate a final value for $\Delta n_u(\lambda, T, P = 1$ atm$)$ of O_2 of 6.6×10^{-25} m^2 V^{-2}. The error exceeds 50%. The value of reference [9], as reported in [8], corresponds at the same conditions to 5.2×10^{-25} m^2 V^{-2} with an error bar also far exceeding 50%. Our values and these previous data are in agreement within the error bars.

We have reported theoretical estimates at different wavelengths. As for $\lambda = 514.5$ nm an experimental value at 1 atm and room temperature is published in reference [7]. It corresponds to $4.2 \pm 0.1 \times 10^{-25}$ m^2 V^{-2}, 15% larger than our estimate of 3.6×10^{-25} m^2 V^{-2} atm^{-1}, see Table 4. A somewhat historical value at $\lambda = 650$ nm published in 1936 by Breazeale [10] is also reported in reference [7]. It corresponds to $5.0 \pm 0.2 \times 10^{-25}$ m^2 V^{-2} at room temperature and 1 atm. This value also is slightly larger than our estimate of Table 4.

We thank A. Arie, G. Rikken and J. Vigué, for their scientific interest and support.

References

1. J. Kerr, Phil. Mag. **4**, 337 (1875)
2. J. Kerr, Phil. Mag. **4**, 416 (1875)
3. C.J.F. Böttcher, P. Bordewijk, *Theory of Electric Polarization, Dielectric in time–dependent fields* (Elsevier, Amsterdam, 1978), Vol. II
4. A.D. Buckingham, Proc. Phys. Soc. A **68**, 910 (1955)
5. A.D. Buckingham, Proc. Roy. Soc. A **267**, 271 (1962)
6. A.D. Buckingham, Proc. Phys. Soc. A **68**, 905 (1955)
7. S. Carusotto, E. Iacopini, E. Polacco, F. Scuri, G. Stefanini, E. Zavattini, Nuovo Cim. D **5**, 328 (1985)
8. E. Inbar, A. Arie, Appl. Phys. B **70**, 849 (2000)
9. A.A. Mak, O.A. Orlov, V.I. Ustyugov, Sov. J. Quant. Electron. **12**, 1574 (1982)
10. W.M. Breazeale, Phys. Rev. **48**, 237 (1935)
11. C. Hermans, A.C. Vandaele, S. Fally, M. Carleer, R. colin, B. Coquart, A. Jenouvrier, M.F. Merienne, Absorption cross-section of the collision-induced bands of Oxygen from the UV to the NIR, in *Weakly Interacting Molecular Pairs: Unconventional Absorbers of Radiation in the Atmosphere*, edited by C. Camy-Peyret, A.A. Vigasin (Kluwer Academic Publishers, Netherlands, 2003), p. 193
12. A.R.W. McKellar, N.H. Rich, H.L. Welsh, Can. J. Phys. **50**, 1 (1972)
13. V.I. Dianov-Klokov, Opt. Spectr. **20**, 530 (1966)
14. R. Klotz, C.M. Marian, S.D. Peyerimhoff, B.A. Hess, R.J. Buenker, Opt. Spectr. **89**, 223 (1984)
15. D. Spelsberg, W. Meyer, J. Chem. Phys. **101**, 1282 (1994)
16. W. Rijks, M. van Heeringen, P. Wormer, J. Chem. Phys. **90**, 6501 (1989)
17. Y. Luo, H. Ågren, B.F. Minaev, P. Jörgensen, J. Mol. Structure (Theochem) **336**, 61 (1995)
18. B.F. Minaev, Phys. Chem. Chem. Phys. **1**, 3403 (1999)
19. D. Spelsberg, W. Meyer, J. Chem. Phys. **109**, 9802 (1998)
20. B.F. Minaev, Spectrochim. Acta A **60**, 1027 (2004)
21. P. Neogrády, M. Medved, I. Cernusák, M. Urban, Mol. Phys. **100**, 541 (2002)
22. A. Cotton, M. Mouton, Compt. Rend. **141**, 317 (1905)
23. A.D. Buckingham, J.A. Pople, Proc. Phys. Soc. B **69**, 1133 (1956)
24. C. Rizzo, A. Rizzo, D.M. Bishop, Int. Rev. Phys. Chem. **16**, 81 (1997)
25. D. Jonsson, P. Norman, O. Vahtras, H. Ågren, A. Rizzo, J. Chem. Phys. **106**, 8552 (1997)
26. D.M. Bishop, P. Norman, Calculation of dynamic hyperpolarizabilities for small and medium sized molecules, in *Handbook of Advanced Electric and Photonic Materials and Devices, Nonlinear Optical Materials*, edited by H.S. Nalwa (Academic Press, San Diego, 2000), Chap. 1, Vol. 9

27. R.W.P. Drever, J.L. Hall, F.V. Kowalsky, J.H. amd, G.M. Ford, A.J. Munley, H. Ward, Appl. Phys. B **31**, 97 (1983)
28. G. Cantatore, F.D. Valle, E. Milotti, P. Pace, E. Zavattini, E. Polacco, F. Perrone, C. Rizzo, G. Zavattini, G. Ruoso, Rev. Sci. Instrum. **66**, 2785 (1995)
29. The vacuum chamber was kindly given to us by A. Arie and it is the one also used in reference [8]
30. G.L.J.A. Rikken, C. Rizzo, Phys. Rev. A **63**, 012107 (2000)
31. R.C. Jones, J. Opt. Soc. Am. **38**, 671 (1948)
32. F. Brandi, F. della Valle, A.M. de Riva, P. Micossi, F. Perrone, C. Rizzo, G. Ruoso, G. Zavattini, Appl. Phys. B **65**, 351 (1997)
33. F.A. Korolev, A.Y. Klementéva, Fizika. **35**, 42 (1980)
34. J. Olsen, P. Jørgensen, Time-dependent response theory with applications to self-consistent field and multiconfigurational self-consistent field wave functions, in *Modern Electronic Structure Theory*, edited by D.R. Yarkony (World Scientific, Singapore, 1995), Part II, p. 857
35. J. Olsen, P. Jørgensen, J. Chem. Phys. **82**, 3235 (1985)
36. D.M. Bishop, Rev. Mod. Phys. **62**, 343 (1990)
37. D.M. Bishop, B. Kirtman, J. Chem. Phys. **95**, 2646 (1991)
38. D.M. Bishop, P. Norman, J. Chem. Phys. **111**, 3042 (1999)
39. T.H. Dunning, J. Chem. Phys. **90**, 1007 (1989)
40. R.A. Kendall, T.H. Dunning, R.J. Harrison, J. Chem. Phys. **96**, 6796 (1992)
41. T. Helgaker, P. Jørgensen, J. Olsen, *Molecular Electronic-Structure Theory* (Chichester, New York, 1999)
42. Y. I'Haya, F. Matsukawa, Int. J. Quant. Chem. Symp. **7**, 181 (1973)
43. P.H. Krupenie, J. Phys. Chem. Ref. Data **1**, 423 (1972)
44. K. Andersson, M.R.A. Blomberg, M.P. Fülscher, G. Karlström, R. Lindh, P.Å. Malmqvist, J. Olsen, B.O. Roos, A.J. Sadlej, M. Schütz, L. Seijo, L. Serrano-Andrés, P.E.M. Siegbahn, P.O. Widmark, *MOLCAS Version 4* (Lund University, Sweden, 1997)
45. T. Helgaker, H.J.A. Jensen, P. Jørgensen, J. Olsen, K. Ruud, H. Ågren, A.A. Auer, K.L. Bak, V. Bakken, O. Christiansen, S. Coriani, P. Dahle, E.K. Dalskov, T. Enevoldsen, B. Fernandez, C. Hättig, K. Hald, A. Halkier, H. Heiberg, H. Hettema, D. Jonsson, S. Kirpekar, R. Kobayashi, H. Koch, K.V. Mikkelsen, P. Norman, M.J. Packer, T.B. Pedersen, T.A. Ruden, A. Sanchez, T. Saue, S.P.A. Sauer, B. Schimmelpfennig, K.O. Sylvester-Hvid, P.R. Taylor, O. Vahtras, DALTON, *an ab initio electronic structure program, Release 1.2*, 2001 see `http://www.kjemi.uio.no/software/dalton/dalton.html`
46. N.J. Bridge, A.D. Buckingham, Proc. R. Soc. Lond. A **295**, 334 (1966)
47. A. Kumar, W.J. Meath, P. Bündigen, A.J. Thakkar, J. Chem. Phys. **105**, 4827 (1996)
48. S.A.C. McDowell, W.J. Meath, Can. J. Chem. **76**, 483 (1998)
49. B. Fernández, C. Hättig, H. Koch, A. Rizzo, J. Chem. Phys. **110**, 2872 (1999)
50. H. Koch, C. Hättig, H. Larsen, J. Olsen, P. Jørgensen, B. Fernández, A. Rizzo, J. Chem. Phys. **111**, 10108 (1999)
51. C. Hättig, J. López Cacheiro, B. Fernández, A. Rizzo, Mol. Phys. **101**, 1983 (2003)